

See discussions, stats, and author profiles for this publication at: <https://www.researchgate.net/publication/348836585>

Investigating a Laser-Induced Titanium Plasma Under an Applied Static Electric Field

Article in Spectroscopy · January 2021

CITATIONS

3

READS

219

9 authors, including:



Emmanuel Asamoah

Jiangsu University

14 PUBLICATIONS 55 CITATIONS

[SEE PROFILE](#)



Kwaku Ayepah

Jiangsu University

7 PUBLICATIONS 50 CITATIONS

[SEE PROFILE](#)



Samuel Britwum Wilson

Jiangsu University

2 PUBLICATIONS 3 CITATIONS

[SEE PROFILE](#)

Some of the authors of this publication are also working on these related projects:



EFFECTS OF SOLAR FLUX, TEMPERATURE, CURRENT, VOLTAGE, SPEED OF WIND AND TIME VARIATION AND THE EFFICIENCY OF THE SOLAR PV ON A DC COMPRESSOR [View project](#)



DETECTION OF LOTUS ROOT CONTAMINANTS USING INTELLIGENT VISUAL MACHINE VISION TECHNIQUES [View project](#)

PEER-REVIEWED RESEARCH

Spectroscopy papers have undergone a double-blind peer review process and are available on our open-access website.

Investigating a Laser-Induced Titanium Plasma Under an Applied Static Electric Field

Emmanuel Asamoah, Yao Hongbing, Wei Pengyu, Cong Jiawei, Zhu Weihua, Zhang Lin, Anita Asamoah, Kwaku Ayepah, and Samuel Britwum Wilson

We investigate the effect of an applied electric field on the laser-induced titanium plasma. We employed a Q-switched Nd:YAG laser system with a wavelength of 1064 nm and focused on the surface of the titanium target. We observed that the intensities of the negative biasing voltages were higher than those of the positive biasing voltages. We recorded an enhancement in the intensity 2.5 times higher with the -15 kV voltage compared to one without. With an applied electric field of 15 kV, the spectral intensity of the titanium plasma recorded a 0.9 times decrease in the intensity with reference to the zero voltage. The electrical characterization of the titanium plasma was also investigated. The results showed a sharp decrease in the electrical signal as the distance between the plates increased from 15 to 60 mm. From the Saha-Boltzmann equation, the plasma temperature was calculated at 9152 K with a laser energy of 100 mJ and an applied electric field of -15 kV. The plasma temperatures were enhanced under the negative biasing voltage case compared to the positive biasing voltage case. The electron density of the titanium plasma was also examined, and the results predicted increasing electron density with increasing laser energy. At an applied electric field of -15 kV and laser energy of 300 mJ, the highest electron density of the titanium plasma was recorded as $1.51 \times 10^{18} \text{ cm}^{-3}$.

Laser induced breakdown spectroscopy (LIBS) is a quantitative analytical technique that employs a high-power laser beam focused on the surface of a target, which then ablates the surface of the target. This process is carried out to investigate the elemental composition of the target material. The spectra analysis gives detailed information about the composition of the target sample. This technique and its applications have been used in many scientific fields and industries (1–11) such as material sciences, analytical chemistry and plasma physics (12–14). Researchers all over the world who work in the field of LIBS have studied the potential of the LIBS technique for the analysis (15,16) of different target samples such as liquids (17), solids (18), and gasses (19–23). The LIBS technique has numerous advantages compared to other spectroscopic techniques such as inductively coupled plasma-atomic emission spectroscopy (ICP-AES) and atomic absorption spectroscopy (AAS) (24–26). These advantages include in situ analysis and little or no sample preparation (27, 28). The analytical performance of the plasma mostly depends on several plasma parameters such as the laser fluence, the pulse repetition rate, and the wavelength (29). In LIBS, the plasma expansion and the plasma parameters, such as electron temperature and density, can also be in-

fluenced by other experimental conditions, such as the nature of the ambient environment, laser wavelength, the applied laser energy (30–34), the presence of cavity confinement, and the applied electric field.

In our previous paper (9), we studied the influence of laser energy on the laser-induced magnesium plasma. The results showed that the laser energy had a huge effect on the electron temperature. We also reported a study (35) on the influence of cavity and magnetic confinements on the signal enhancement of a laser-induced magnesium and titanium plasmas. The study employed both circular and square cavities to investigate the confinement effect on the spectral intensities of the plasmas. The spectra intensities of both the circular and square cavities were more enhanced when compared with the cavity-free case.

Few papers have been reported on the laser-induced plasma under applied electric fields. Robledo-Martinez and his team (36) investigated on the dipolar field and plasma expansion of a laser-induced breakdown in a uniform DC field. They focused an Nd:YAG laser between two parallel plates connected to a DC power supply and investigated the plasma expansion and formation of the LIBS in air by utilizing an electric

field measurement and fast photography. Their results predicted that the plasma produces a dipolar electric field that is proportional to the strength of the bias. They reported that the dipole was caused by the redistribution of the charges over the surface of the plasma.

Elhassan and his group (37) also studied the effect of applying static electric field with different polarities on the laser-induced plasma parameters. Their work revealed an enhancement in the signal-to-noise (S/N) ratio of both the neutral and ionic lines of the aluminum plasma under forward biasing voltage. They also recorded a decrease in the emission intensities of the plasma in the case of reverse biasing of the voltage.

Alvarez and his coauthors (38) published a report on the spectral and electrical characterization of laser produced plasma. They studied the influence of transverse electric field produced by two parallel capacitor plates on the aluminum target. Their results showed that the electron temperature and density are directly proportional to the applied laser energy. They also recorded that the electric signal as a function of the distance of separation of the plates had a relationship, which is approximately the inverse of the square of the distance.

We present an in-depth study on the titanium plasma under static electric field by analyzing the plasma parameters of the titanium plasma. The aims of this study are to investigate the effect of the electric field on the electron temperature and density of the titanium plasma and also to study the electrical characterization of the titanium plasma.

Materials and Methods

The experimental set-up in this work is similar to the report of (37, 38). Figure 1a shows the experimental setup for the laser-induced plasma. The plasma was produced by a Q-switched Nd:YAG laser operating with a laser pulse of 100 mJ/pulse, with a pulse duration of 8 ns at its fundamental wavelength of 1064 nm. An energy meter

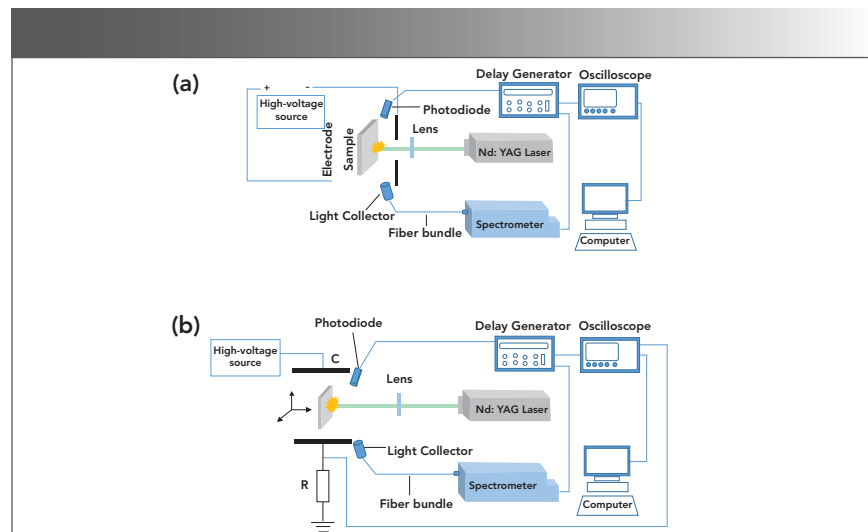


FIGURE 1: (a) The schematic diagram of the experimental setup of the laser-induced plasma for the electric field confinement. (b) The setup to study the electrical characterization of the titanium plasma (where C is a capacitor and R is a resistor).

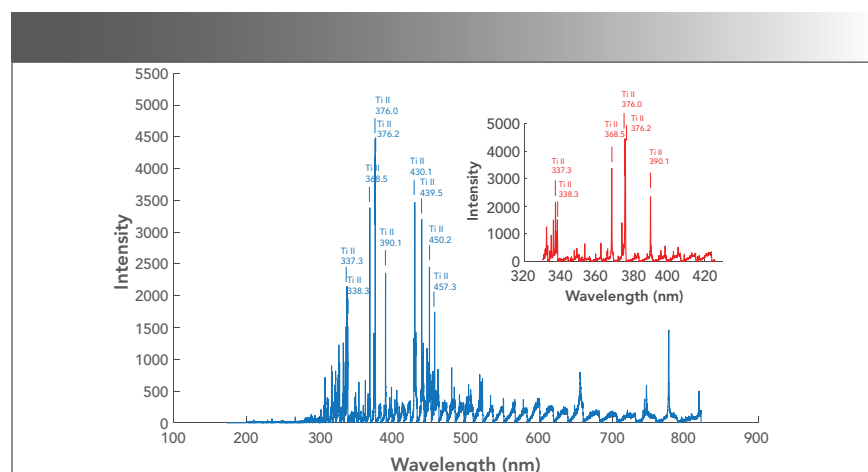


FIGURE 2: The emission spectra of titanium with an applied electric field of -15 kV in the spectral region of 200–800 nm, with a laser energy of 100 mJ.

TABLE I: The spectroscopic data of the titanium (Ti) spectral lines acquired from the NIST database (43).

Spectral Line	λ_{nm} (nm)	E_m (eV)	A_{mn}	g_m
Ti I	336.2	5.99	1.58	9
Ti I	390.1	3.20	0.01	7
Ti I	430.1	3.72	0.16	7
Ti II	337.3	1.41	3.69	8
Ti II	368.5	3.97	0.00	6
Ti II	376.0	3.90	0.94	8
Ti II	376.2	5.89	0.22	8
Ti II	439.4	4.04	0.01	4
Ti II	450.1	3.87	0.09	6

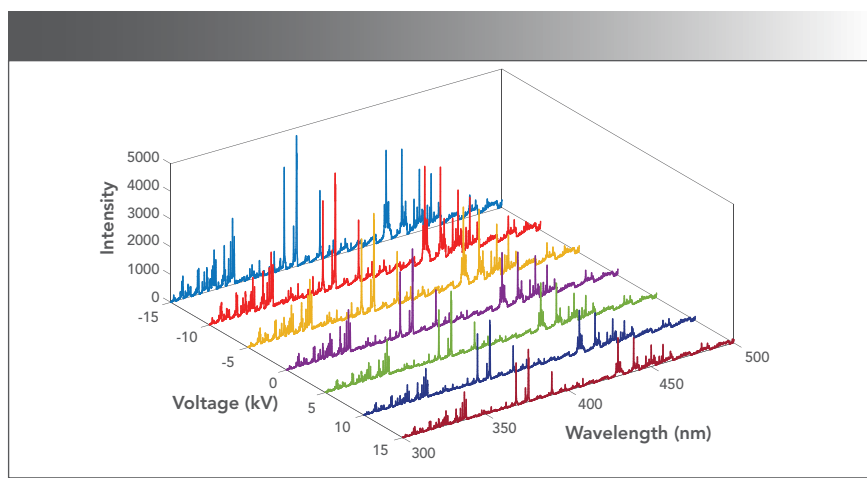


FIGURE 3: A three-dimensional plot of the emission spectra of titanium under different applied electric fields ranging from -15 kV to +15 kV, in the spectral region of 300–500 nm, with a laser energy of 100 mJ.

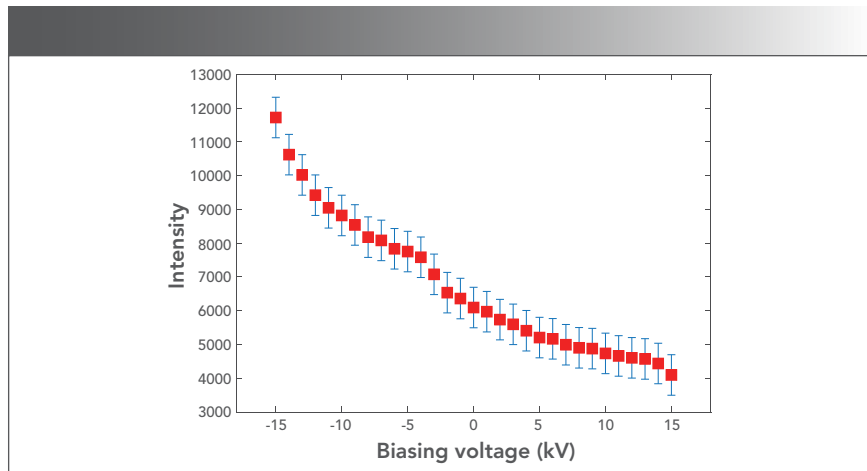


FIGURE 4: A plot of the intensities of the titanium II – 376.0 nm lines against the negative and positive biasing voltages at a laser energy of 150 mJ.

(Nova II, Ophir from Laser Measurement Group, Ophir Optronics Ltd.) was used to monitor the shot-to-shot laser pulse energy. The pulse laser beam was focused on the titanium target by a plano-convex lens with a focal length of 15 cm. The target was a highly polished titanium plate with 99.9% purity. The target was sandwiched between two polished copper plates at 2 cm apart. These copper plates were used as the electrodes for the application of the voltage. The diameter of the two electrodes was 50 mm with a thickness of 5 mm. The electrode between the focusing lens and the target sample had a hole with a diameter of 5 mm at the center to allow the focusing of the laser beam on the target surface. To

increase the S/N ratio and the reproducibility of the measurements, the collection of the spectra data was done by averaging 15 single accumulations of spectra from 15 different fresh positions on the target surface. The voltage across the electrodes was varied from 0 to 15 kV to study the electric field effect on the plasma. The polarities of the electrodes were also reversed to further study their effect on the plasma. The spectra were collected by a fiber bundle coupled with an echelle spectrometer (Andor Technology, Mechelle 5000. Wavelength range of 200–975 nm, wavelength accuracy of ± 0.05 nm, focal length of 195 mm and high resolution power up to 6000 and with spectral resolution of $\lambda/\Delta\lambda=5000$) with an

inbuilt ICCD camera. The delay generator was also employed to vary the delay time (Stanford Research System, model DG645).

The setup in Figure 1b was used to study the electrical characterization of the titanium target. The capacitor plates were connected parallel to the laser beam. One of the plates was connected to the ground through a $5.0\text{ k}\Omega$ resistor, and the other plate was connected to a high voltage source. The voltage source varied from 0 to 15 kV, and the distance between the two plates varied between 15 mm to 60 mm with an interval of 5 mm. The titanium sample was sandwiched between the two capacitor plates, and was affixed to a translation stage to enable fresh positions for the focusing of the laser beam onto the titanium target. The spectra from the emission were collected by a fiber bundle which was coupled with an echelle spectrometer with an inbuilt intensified charged coupled device (ICCD) camera (1024×1024 pixels iStar from Andor Technology). The ICCD was triggered by a photodiode in order to synchronize the delay time between the laser pulse and the ICCD. The analysis of the data was performed by a computer with Andor software (Andor Solis, Andor Technology).

Results and Discussion

Spectral Emission Intensity

To investigate the influence of static electric fields on the titanium plasma, we studied the spectral analysis of the laser-induced plasma. The spectral emission of the plasma was recorded under several experimental conditions. Figure 2 shows the emission spectra of the LIBS plasma obtained with a laser energy of 100 mJ at atmospheric pressure in the presence of an applied electric field. The emission spectra revealed the spectral lines of titanium I at 336.2 nm, 390.1 nm, 430.1 nm and titanium II at 337.3, 368.5, 376.0, 376.2, 439.5 and 450.2 nm. From the emission spectra, we observed a strong continuum with an increase in the laser energy. Varying the electric field resulted in an increase of the spectral intensities of the plasma. Also in the early stage of the plasma generation, the signal was mostly dominated by the continuum emission, which was because

of the collision of the ions and atoms with the electrons.

The Electric Field Effect on the Plasma

Figure 3 depicts a three-dimensional plot of the emission spectra generated by an Nd:YAG laser operating with a laser energy of 100 mJ and a delay time of 15 ns under different applied electric fields by forward and reverse biasing of the electrodes. The figure reflects a wide titanium spectral range from 300–500 nm. It also depicts the spectra intensity differences between the negative biasing voltages and the positive biasing voltages. After observing the peak intensities of both the negative and positive biasing cases, we found the intensities of the negative biasing voltages were much higher than that of the positive biasing voltages. We also found that the intensities of both the ionic and atomic spectral lines were all influenced by the applied electric fields. We conducted thorough investigations on the obtained spectra, and plotted the intensities of the Ti II-376.0 nm against the biasing voltages from -15 to 15 kV as shown in Figure 4. The plot reveals an enhancement in the Ti II-376.0 nm lines in the forward biasing case. Comparing the zero voltage intensity with the -15 kV voltage case, we observed a 2.5 fold increase in the intensity of the -15 kV voltage. After reversing the polarities of the applied electric field, the 15 kV voltage case we recorded a 0.9 times decrease in the intensity with reference to the zero voltage. These decreases in the intensities can be attributed to the decrease in the recombination rate, the strong attractive field between the negative front electrode, and the positive ions within the plasma. The intensity enhancement of the titanium II-376.0 nm lines via the forward biasing case was a result of the repulsive fields between the positive front electrodes and the positive ions within the plasma.

Electrical Characterization of the Titanium Plasma

The setup in Figure 1b was used to investigate the electrical characterization of the titanium plasma produced in air at atmospheric pressure. The oscilloscope was used to monitor and study the electrical

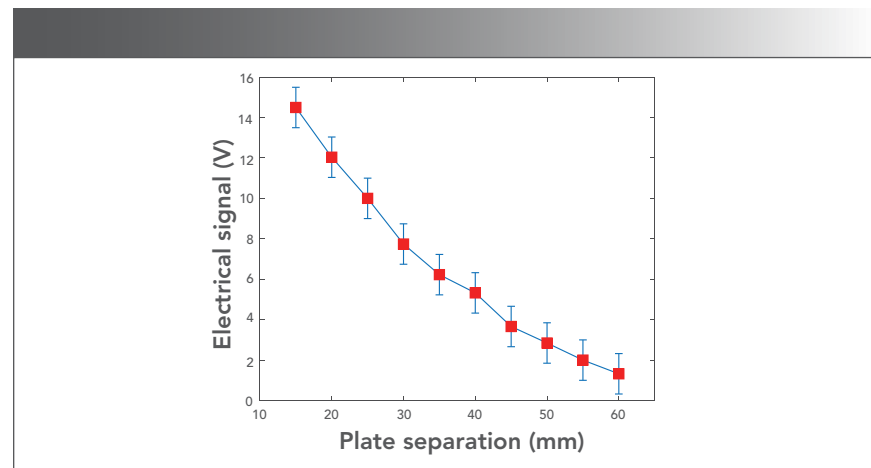


FIGURE 5: A plot of the electrical signal as a function of the distance of separation (in mm) between the capacitor plates.

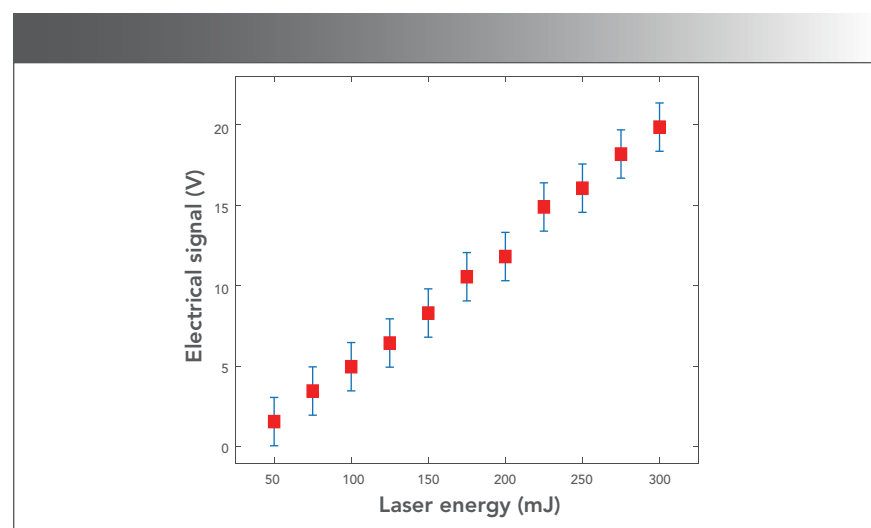


FIGURE 6: A plot of the electrical signal as a function of the applied laser energy.

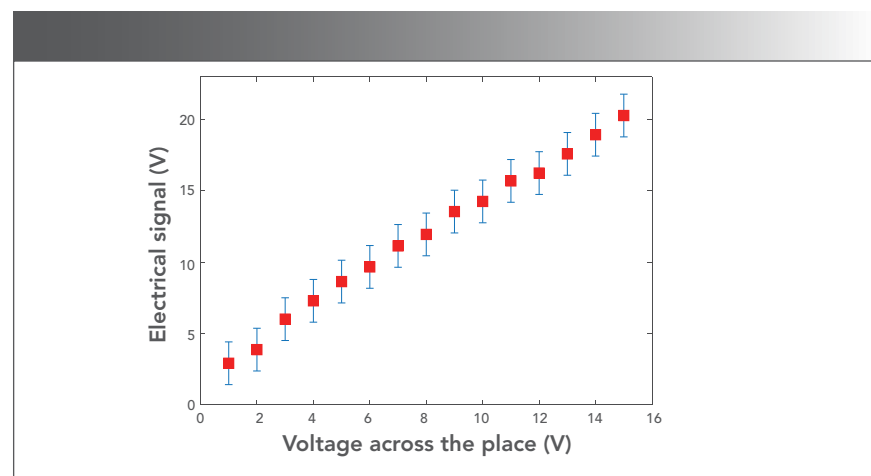


FIGURE 7: A plot of the electrical signal as a function of the applied voltage (V) across the capacitor plates.

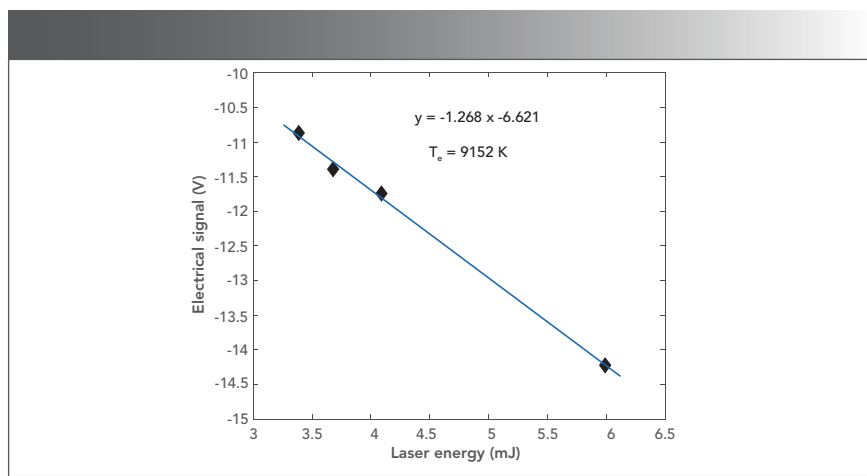


FIGURE 8: The Saha-Boltzmann plot using the titanium lines at a laser energy of 100 mJ with an applied electric field of -15 kV.

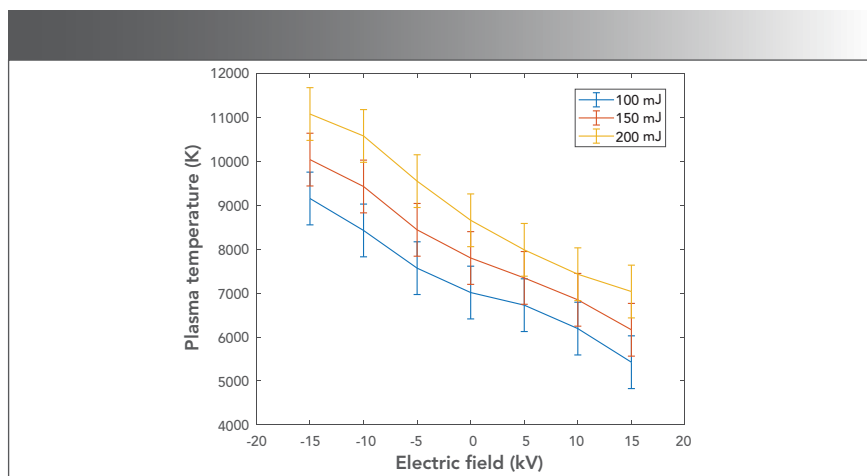


FIGURE 9: A plot of plasma temperature against applied electric field with three different laser energies of 100, 150 and 200 mJ.

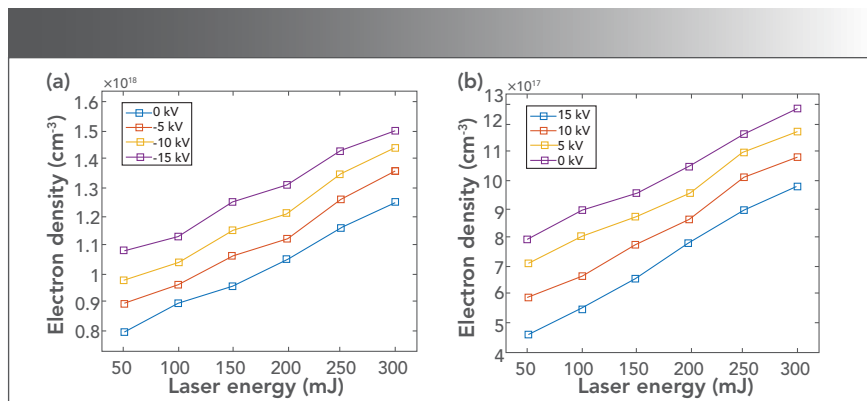


FIGURE 10: (a) A plot of electron density against laser energy with applied electric field under negative biasing voltage (b) A plot of electron density against laser energy with an applied electric field under positive biasing voltage.

signals generated from the plasma. During the process of plasma formation within

the two capacitors, an electric pulse was generated, which can be measured as a

potential difference across the resistor connected to the ground. We further characterize these electrical signals as a function of the laser energy and the distance of separation between the two capacitor plates.

From Figure 5, we observed that as the distance of separation between the two capacitors increased, the electrical signals decreased. The highest electrical signal was recorded with a distance of separation between the plates as 15 mm. From these results, we found that there was a sharp decrease in the electrical signal as the distance between the plates increased from 15–60 mm. Figure 6 depicts the electrical signals as a function of the laser energy. As can be seen from the figure, the electrical signals increase with increasing laser energy. At a laser energy of 300 mJ the maximum electrical signal was recorded as 18.2 V. We also observed a linear relationship between the electrical signals and the laser energies. The plotting of the electrical signal against the applied voltage across the capacitor plates is presented in Figure 7. We also observed a linear relationship between the electrical signals and the applied voltages. It can be seen that the electrical signals increase with increasing voltage across the capacitor plates. From the Saha-Boltzmann equation, plotting the expression at the right-hand side of the equation (E_m) against the expression in the left-hand side of the equation (in equation 2b), gives a linear fit with a slope which is equal to $-1/(k_B T)$. Where k_B and T are the Boltzmann's constant and the plasma temperature respectively. Using the spectroscopic parameters of the titanium spectra lines acquired from the NIST database as shown in Table I. The plasma temperature can be deduced from the slope of the Saha-Boltzmann plot as depicted in Figure 8.

Determination of Electron Temperature Saha-Boltzmann Plot Method

The plasma temperature of the laser-induced titanium plasma with and without applied electric field can be deduced from the Saha-Boltzmann equation used in our previous work (35).

$$\ln\left(\frac{I_1 \lambda_1}{g_1 A_1}\right) = -\frac{1}{kT} E_k^1 + \ln\left(hc \frac{N_e}{Z_0(T)}\right) \quad [1]$$

$$\ln\left(\frac{I_2 \lambda_2}{g_2 A_2}\right) - \ln\left(\frac{2(2\pi mk)(3/2)T^{3/2}}{h^3 N_e}\right) = -\frac{1}{kT} \times (E_k^2 + E_{IP}) + \ln\left(hc \frac{N_e}{Z_0(T)}\right) \quad [2a]$$

$$\left(\ln\left(\frac{I_{mn} \lambda_{mn}}{A_{mn} g_{mn}}\right)\right) \quad [2b]$$

where E_{IP} is the ionization energy (eV), N_0 , N_e and $Z_0(T)$ represents the particle density, electron density and the partition function respectively. c , m , and A denotes the speed of light, mass of the electron and the ionic broadening parameter respectively. T is the plasma temperature, and h is the Planck's constant.

From the neutral and the ionic lines for the titanium spectra lines, we employ the Saha-Boltzmann plot method to calculate the plasma temperature of the laser-induced plasma. Equations 1 and 2a can be used to express the neutral and the ionic lines respectively (39–42).

From the Saha Boltzmann plot, the plasma temperature was calculated to be 9152 K with a laser energy of 100 mJ and an applied electric field of -15 kV. With the same laser parameters, the plasma temperature of the titanium plasma with an applied electric field of -5 and -10 kV was found to be 7567 and 8425 K respectively. Also, for the positive biasing voltage case with an applied electric field of 5, 10 and 15 kV with a laser energy of 100 mJ, the plasma temperatures of the titanium plasma were found to be 6725, 6192, and 5427 K, respectively.

Figure 9 represents a plot of plasma temperature against applied electric field with different laser energies. The plasma temperature of the titanium plasma without electric field was recorded to be 7012 K at a laser energy of 100 mJ. From Figure 9, we can see that the plasma temperature increases with increasing laser energy under both positive and negative biasing voltages. However, comparing the positive and negative biasing voltages, the plasma temperatures of the negative biasing cases were more enhanced as compared to the positive biasing cases. Comparing the plasma temperatures of the positive biasing cases with the case without electric field, it was observed that the plasma temperature decreases in the presence of positive electric fields. At an applied electric field of -15 kV and a laser energy of 200 mJ the plasma temperature was found to be 11274 K. Also, for the positive biasing voltage of 15 kV at the same laser energy of 200 mJ, the plasma temperature was also calculated to be 7035 K. Figure 9 shows that the plasma temperature drops tremendously from the negative biasing voltage of -15 kV to positive biasing voltage of 15 kV.

Electron Density

In this section, we discuss the effect of the applied electric field on the electron density of the titanium plasma. The electron density can be calculated by using the full width at half maximum (FWHM) of the spectral lines, which can be expressed as:

$$\Delta\lambda_{1/2}(nm) = 2\omega \left(\frac{N_e}{10^{16}}\right) + 3.5A \left(\frac{N_e}{10^{16}}\right)^{1/4} \left[1 - \frac{3}{4} N_D^{-1/3}\right] \omega \left(\frac{N_e}{10^{16}}\right) \quad [3]$$

where N_D is the number of particles in the Debye sphere, N_e is the electron density, ω and A are the electron impact width parameter and ionic broadening parameter respectively. Ignoring the contribution of the ionic broadening, the expression in equation 3 can be written as (35, 39):

$$\Delta\lambda_{1/2}(nm) = 2\omega \left(\frac{N_e}{10^{16}}\right) \quad [4]$$

A plot of the electron density against the laser energy at different applied electric fields under negative biasing of the voltage is depicted in Figure 10a. The graph reveals the general trend of increasing electron density with increasing laser energy. The electron density of the titanium plasma at a laser energy of 100 mJ at an applied electric field of -5 kV was deduced to be $9.61 \times 10^{17} \text{ cm}^{-3}$. At an applied electric field of -15 kV and laser energy of 300 mJ, the highest electron density of the titanium plasma was recorded as $1.51 \times 10^{18} \text{ cm}^{-3}$. Figure 10b also represents a plot of electron density against laser energy with an applied electric field under positive biasing voltage. Comparing the electron density of the negative biasing case with the positive biasing case, we observed that the electron density increases tremendously under the negative biasing case. The minimum electron density was obtained as $4.66 \times 10^{17} \text{ cm}^{-3}$ under the positive biasing of the voltage at a laser energy of 50 mJ.

Conclusion

In this study, we presented the investigation of the effect of applied static electric fields on the plasma parameters of a laser-induced titanium plasma. The study employed an Nd:YAG laser operating at its fundamental wavelength of 1064 nm focused on the surface of the titanium target. Applying static electric fields through forward and reverse biasing of the electrodes. We found that the intensities of the negative biasing voltages were much higher than those of the positive biasing voltages. It was also found that the intensities of both the ionic and atomic spectral lines were all influenced by the applied static electric fields. Comparing the intensity of the case of zero voltage with the -15 kV voltage case, we observed a 2.5 fold enhancement in the intensity of the -15 kV voltage. By reversing the polarities of the applied electric field, we recorded in the 15 kV voltage case a decrease in the intensity by 0.9 times with reference to the zero voltage. The decrease in the spectral intensities of the titanium plasma was attributed to the decrease in the recombination rate, which was as a result of the strong attractive field between the negative front electrode and the positive ions within the plasma. We also studied the electrical characteristics of the plasma and observed that increasing the distance of separation between the two capacitor plates decreases the electrical signals. The highest electrical signal was recorded with a distance of separation between the plates as 15 mm. The plasma temperature was deduced to be 9152 K with a laser energy of 100 mJ with an applied electric field of -15 V. We found that the plasma temperature of the negative biasing cases was more enhanced as compared to the positive biasing cases. The

electron density was also found to be $9.61 \times 10^{17} \text{ cm}^{-3}$ with a laser energy of 100 mJ at an applied electric field of -5 kV. Increasing the applied electric field to -15 kV, the maximum electron density was obtained as $1.51 \times 10^{18} \text{ cm}^{-3}$ at a laser energy of 300 mJ.

Acknowledgments

This work was supported by the National Natural Science Foundation of China (Nos. 51775253, 61505071), the Fundamental Research Funds for the Central Universities (No. 2019B02614), China Postdoctoral Science Foundation (2017M611725).

References

- (1) C.F.B.R. Noll, M. Brunk, S. Connemann, C. Meinhardt, M. Scharun, V. Sturm, J. Makowe, and C. Gehlen, *Spectrochim. Acta. B*, **93**, 41–51 (2014).
- (2) C.F.B.R. Noll, S. Connemann, C. Meinhardt, and V. Sturm, *J. Anal. Atom. Spectrom.* **33**, 945–956 (2018).
- (3) V. S. R. Noll, Ü. Aydin, D. Eilers, C. Gehlen, M. Höhne, A. Lamott, J. Makowe, and J. Vrenegor, *Spectrochim. Acta. B*, **63**, 1159–1166 (2008).
- (4) P. Y. M. W. Rapin, S. Maurice, R. C. Wiens, D. Laporte, B. Chauviré, O. Gasnault, S. Schröder, P. Beck, S. Bender, O. Beysac, A. Cousin, E. Dehouck, C. Drouet, O. Forni, M. Nachon, N. Melikechi, B. Rondeau, N. Mangold, and N. H. Thomas, *Spectrochim. Acta. B*, **130**, 82–100 (2017).
- (5) European Commission, "Critical Raw Materials for the EU, Report of the Ad hoc Working Group on Defining Critical Raw Materials," 85 (2010).
- (6) European Commission, "Critical Raw Materials for the EU, Report of the Ad hoc Working Group on Defining Critical Raw Materials," 41 (2014).
- (7) Y. Fu et al., *Spectrochim. Acta. B*, **155**, 67–78 (2019).
- (8) S.R.N.J. McMillan, K. Kochelek, and C. McManus, *Geostand. Geoanal. Res.* **38**, 329–343 (2014).
- (9) E. Asamoah, and Y. Hongbing, *Appl. Phys. B*, **123**(1), 22 (2017).
- (10) G. Cristoforetti, E. Tognoni, and L. Gizzi, *Spectrochim. Acta. B*, **90**, 1–22 (2013).
- (11) D. W. Hahn and N. Omenetto, *Appl. Spectrosc.* **66**, 347–419 (2012).
- (12) A. Neogi, and R. Thareja, *Phys. Plasmas*, **6**(1), 365–371 (1999).
- (13) L. D. Landau, and E. M. Lifshits, *Fluid mechanics*, by L.D. Landau and E.M. Lifshitz (Pergamon Press, London, 1959).
- (14) Y. B. Z. d. a. Y. P. Raizer, *Physics of Shock Waves and High Temperature Hydrodynamics Phenomena* (Academic Press, New York (1966).
- (15) D. Kim et al., *Appl. Spectrosc.* **51**(1), 22–29 (1997).
- (16) W.T.Y. Mohamed, *Opt. Laser Technol.* **40**(1), 30–38 (2008).
- (17) V. Sturm, L. Peter, and R. Noll, *Appl. Spectrosc.* **54**(9), 1275–1278 (2000).
- (18) A.P. Michel et al., *Appl. Opt.* **46**(13), 2507–2515 (2007).
- (19) D.A. Cremers and L.J. Radziemski, *Anal. Chem.* **55**(8), 1252–1256 (1983).
- (20) L. J. Radziemski and D. A. Cremers, *Laser-induced plasmas and applications* (Marcel Dekker, New York, 1989).
- (21) Y. Lee, K. Song, and J. Sneddon, *Laser induced plasmas for analytical atomic spectroscopy*, (Wiley-VCH: New York, 1997).
- (22) V. Sturm and R. Noll, *Appl. Opt.* **42**(30), 6221–6225 (2003).
- (23) Y.K. Zhang, *Spectrosc. Spec. Anal.* **31**(9), 2542–2545 (2011).
- (24) H. Zhang et al., *Sensors* **19**(19), 4225 (2019).
- (25) D.J. Butcher, *Appl. Spectrosc. Rev.* **41**(1), 15–34 (2006).
- (26) P. Chattopadhyay et al., *Microchimica Acta* **144**(4), 277–283 (2004).
- (27) S. Amoruso et al., *J. Phys. B-At Mol. Opt.* **32**(14), R131 (1999).
- (28) P.C.M. Sababi, *Appl. Spectrosc.* **49**, 499–507 (1995).
- (29) F. Brygo et al., *Appl. Surf. Sci.* **252**(6), 2131–2138 (2006).
- (30) S. Harilal et al., *Appl. Phys. Lett.* **72**(2), 167–169 (1998).
- (31) J. Aguilera and C. Aragon, *Appl. Phys. A* **69**(1), S475–S478 (1999).
- (32) A. Löbe et al., *Anal. Bioanal. Chem.* **385**(2), 326–332 (2006).
- (33) N. M. Shaikh, S. Hafeez, and M. Baig, *Spectrochim. Acta. B* **62**(12), 1311–1320 (2007).
- (34) S. Bashir et al., *Appl. Phys. A* **107**(1), 203–212 (2012).
- (35) E. Asamoah et al., *Laser Part. Beams* 1–12 (2020).
- (36) A. Robledo-Martinez, H. Sobral, and M. Villagrán-Muniz, *J. Phys. D. Appl. Phys.* **37**(20), 2819 (2004).
- (37) A. Elhassan et al., *J. Adv. Res.* **1**(2), 129–136 (2010).
- (38) J. Alvarez, P. Pacheco, and R. Sarmiento, *Journal of Physics: Conference Series* 012009 (2019).
- (39) H. Griem, *Principles of Plasma Spectroscopy* (Cambridge University Press, Cambridge, 1997).
- (40) S. Duixiong et al., *Plasma Sources Sci.T.* **16**(4), 374 (2014).
- (41) H. Yao et al., *Metals* **10**(3), 393 (2020).
- (42) J. Gomba et al., *Spectrochimica Acta Part B*, **56**(6), 695–705 (2001).
- (43) NIST, "Atomic spectra database." http://Physics.nist.gov/PhysRef-Data/ASD-lines_form.html.

Emmanuel Asamoah, Cong Jaiwei, Kwaku Ayepah, and Samuel Britwum Wilson are with the School of Mechanical Engineering at Jiangsu University in Zhenjiang, Jiangsu, China. **Yao Hongbing, Zhu Weihua, and Zhang Lin** are with College of Science at Hohai University in Nanjing, Jiangsu, China. **Wei Pengyu** is with the China Ship Scientific Research Center in Wuxi, Jiangsu, China. **Anita Asamoah** is with the School of Material Science at Jiangsu University of Science and Technology, Zhenjiang, Jiangsu, China. Direct correspondence to: asamoah_grace@hotmail.com; ale-nyao@hhu.edu.cn

